

# Flame Radiation and Liner Heat Transfer in a Tubular-Can Combustor

R. W. Claus,\* G. M. Neely,\* and F. M. Humenik\*  
NASA Lewis Research Center, Cleveland, Ohio

Total and spectral flame radiation measurements were made in a tubular-can combustor at a series of parametric operating conditions to examine the heat transfer within the combustor. Radiation measurements were taken for a range of inlet air pressures of 0.34-2.0 MPa, inlet air temperatures of 533-700 K, with two different fuels, Jet A (13.9% hydrogen) and ERBS (12.9% hydrogen). Measurements of liner temperatures combined with the parametric radiation results allowed a calculation of the combustor liner heat loads. Flame emissivity was determined from the spectral measurements and compared against an empirical correlation.

## Nomenclature

$C$	= convective heat flux
$C_m$	= turbulent mixing coefficient
$D$	= hydraulic diameter
$F$	= film air temperature
$h$	= convective heat-transfer coefficient
$K$	= thermal conductivity
$KC$	= thermal conductive heat flux
$Lu$	= luminosity factor
$M$	= mass flux ratio
$Pr$	= Prandtl number
$R$	= radiation heat flux
$Re$	= Reynolds number
$s$	= slot height
$T$	= temperature
$U$	= velocity
$\alpha$	= absorptivity
$\delta$	= thickness
$\epsilon$	= emissivity
$\rho$	= mass density
$\sigma$	= Stefan-Boltzman constant

## Subscripts

$an$	= annulus conditions
$c$	= casing
$cerm$	= ceramic coating
$eff$	= effective
$f$	= gas film condition at any $x$
$fl$	= flame
$ft$	= flame tube
$H$	= hot-gas conditions
$Hast$	= Hastelloy
$Liner$	= liner average at any $x$
$s$	= film-cooling slot conditions
$T$	= total
$W$	= liner wall
$WA$	= liner wall, annulus side
$WC$	= liner wall at ceramic metal interface
$WH$	= liner wall, flame tube side
$1$	= flux to liner from flame tube side
$2$	= flux from liner to casing side
$3$	= combustor inlet conditions

## Introduction

AN accurate analysis of liner metal temperatures is critical to the determination of combustor liner life. A designer confronting this problem can employ a number of empirical correlations to calculate both the radiative and convective heat loads to the liner. The difficulty arises because not only are these empirical correlations of differing degrees of validity, but also the inputs to these correlations are frequently only assumed. The uncertainty this introduces into the combustor design process can lead to either an overcooling or undercooling of the combustor liner that must be rectified by an increasingly more expensive program of hardware design testing.

Of the empirical correlations used to analyze the liner heat transfer, the greatest uncertainty is generally associated with the prediction of radiative heat transfer. The mechanisms of film cooling are regarded as well understood,<sup>1</sup> but the determination of the local flame emissivity, needed in the calculation of radiative heat transfer, is not firmly defined. The early work of Reeves<sup>2</sup> provided a luminous flame emissivity correlation that is difficult to use and is constructed from data obtained at operating conditions more representative of furnaces than of gas turbine engines. Subsequent work<sup>3-6</sup> has frequently examined only the effect that various parameters have on total radiation. Unfortunately, a total flame radiation measurement cannot distinguish variations in flame emissivity from variations in flame temperature, thereby making it difficult to construct or test flame emissivity correlations.

The purpose of this report is to examine some of the parameters affecting heat transfer to the combustor liner and to test the validity of some of the correlations used in the calculation of liner metal temperatures. Flame emissivities and flame temperatures were determined using a spectral radiometer. These measurements, combined with total radiation and liner temperature measurements, enabled a determination of the local heat loads to the liner. Testing the combustor at a variety of parametric operating conditions permitted examination of some of the factors influencing the heat transfer to the liner. Finally, extrapolation of some of the trends with increasing inlet air temperatures and pressures allows an estimate of the impact that advanced cycle engines will have on liner temperature and durability.

## Apparatus and Procedure

These experiments were conducted with a single JT8D tubular-can combustor installed in a test housing assembly displayed schematically in Fig. 1. Combustor inlet instrumentation consisted of two inlet static pressures and a five-point inlet thermocouple rake located in the inlet plenum section.

Presented as Paper 84-0443 at the AIAA 22nd Aerospace Sciences Meeting, Reno, Nev., Jan. 9-12, 1984; received July 23, 1984; revision received April 1, 1985. This paper is declared a work of the U.S. Government and therefore is in the public domain.

\*Aerospace Engineer.

The combustor exit instrumentation consisted of a set of eight five-point thermocouple rakes for monitoring the exit temperature pattern and a set of four gas-sample probes for exhaust gas analysis. Liner metal temperatures were measured with 24 thermocouples of which 4 were located on the dome and the others divided along opposite sides of the combustor can so that 2 separate thermocouples were on the outside of each cooling louver.

The flame radiation instrumentation consisted of three separate total radiation gages installed at varying axial locations along the combustor housing and a single spectral radiometer positioned in line with the window ports as illustrated in Fig. 2. The three total radiation gages were of a Gardon-type construction with water cooling and a nitrogen purge to insure a clear optical path. The stem of each gage extended to the inner surface of the combustor liner through an existing air entry hole or a specially added clearance hole. The measurement locations corresponded nominally to the primary, secondary, and tertiary combustion zones of the JT8D combustor.

The spectral radiometer system components included an optical sensing head unit, a programmable controller, and a printer as shown in Fig. 3. The sensing head consisted of an optical sighting system, a variable spectral filter, and an indium antimonide radiation detector cooled to the boiling point of liquid nitrogen through a high-pressure cryostat. A programmable controller was used to set the spectral filter at the desired wavelength increments. The spectral filter provided data over a range of wavelengths of 1.5-5.5  $\mu\text{m}$ . Further details of the spectral radiometer are given in Ref. 7, with the only significant difference being the optical view path. Previous experiments employed a traversing mirror. In this experiment, the radiometer optical head was individually sighted through each sapphire window port. The optics of the radiometer were sighted along a 3 mrad field of view focused at infinity. This established uniform detector sensitivity over the hot-gas optical path.

Calibration tests of the spectral radiometer were performed using a high-temperature (1270 K) blackbody. Calibration at several temperatures demonstrated a spectral calibration error of less than 2%. The total radiometers were also checked in this manner, establishing that the Gardon-type total radiometers displayed a fairly uniform spectral response. Under the operational conditions presented herein, the calibration of the total radiometer was not affected by the temperature and wall boundary conditions.

Radiation measurement locations, both total and spectral, are shown in Fig. 4.

The arrangement of the apparatus in the test facility is shown in Fig. 5. The exit instrumentation rakes and gas-sample probes are on the left. The flow direction is right to left. The spectral viewing ports contained sapphire windows whose transmittance bandwidth and high-temperature capability were suited to this application. For safety reasons, local sighting of the spectral detector optics was conducted at

Table 1 Test conditions

Combustor pressure		Combustor inlet temperature		Airflow rate	
MPa	psia	K	°F	kg/s	lb/s
0.34	50	533	500	1.69	3.72
.69	100	533	500	3.37	7.44
1.38	200	533	500	6.75	14.88
2.07	300	533	500	10.12	22.32
0.69	100	616	650	3.14	6.92
1.38	200	616	650	6.28	13.84
2.07	300	616	650	9.42	20.76
0.69	100	700	800	2.95	6.50
2.07	300	700	800	8.84	19.50

Table 2 Fuel characteristics

Specifications	Jet A	ERBS
ASTM distillation, K		
Initial boiling point	411	435
10% evaporated	451	461
50% evaporated	479	488
90% evaporated	517	552
Final boiling point	531	601
Specific gravity at 289 K	0.8142	0.8381
Freezing point, K	226	244
Viscosity at 250 K, $\text{m}^2/\text{s}$	$5 \times 10^{-6}$	$7.2 \times 10^{-6}$
Net heat of combustion, J/g	43 304	42 200
Hydrogen, wt%	13.9	12.9
Aromatics, vol%	17.2	28.8
Sulfur (total), wt%	0.020	0.065

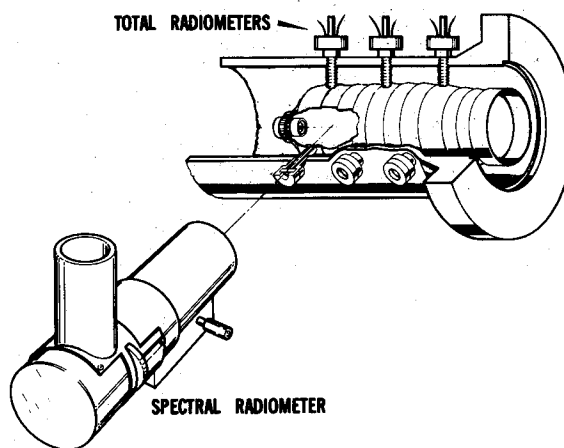


Fig. 2 Assembly of tubular combustor for flame radiation studies.

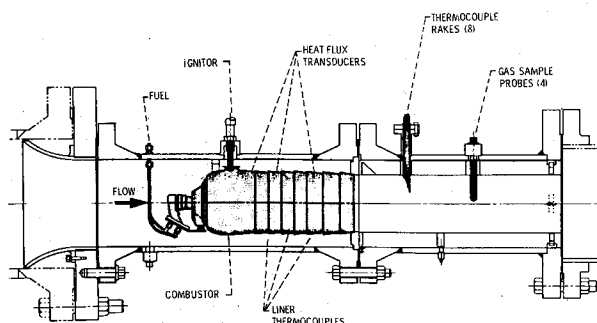


Fig. 1 Schematic of tubular combustor installation. Nominal flow capabilities of test facility: 25 atm inlet pressure, 870 K inlet air temperature, 10 kg/s inlet airflow rate.

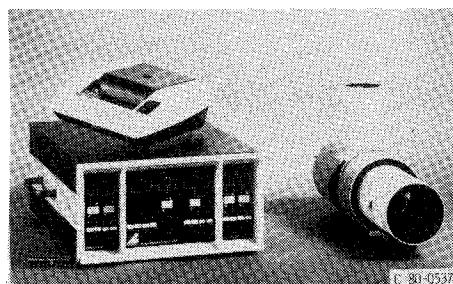


Fig. 3 Spectral radiometer system components: programmable controller with printer and sensing head.

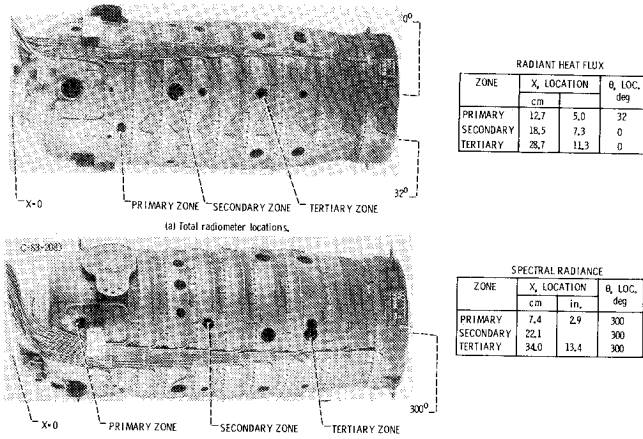


Fig. 4 Tubular-can combustor with flame radiation zone locations.

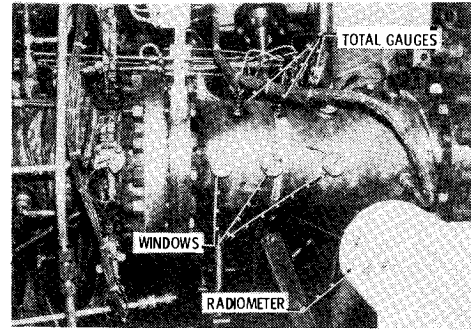


Fig. 5 JT8D combustor housing assembly during experiments showing installation of radiant heat flux transducers, location of window-stations and spectral radiometer sensing head.

low pressure (0.34 MPa). Spectral data scanning and recording was initiated from an adjacent control room.

Test conditions (see Table 1) were selected to cover the normal range of combustor operation while maintaining a constant reference velocity (15 m/s). This maintained similar internal combustor air velocities to minimize aerodynamic effects on the parametric results.

The characteristics of the two fuels used in this investigation are given in Table 2. The specifications for the experimental referee-broadened specification (ERBS) fuel was established in Ref. 8. It was proposed that such a fuel could be produced from the available petroleum stocks without excessive processing costs. Accordingly, the viscosity and boiling points of the ERBS fuel were higher than those for the more fully refined Jet A fuel.

### Heat-Transfer Analysis

This heat-transfer analysis closely follows the approach detailed in Ref. 9. Heat fluxes to and from the combustor liner are treated in a one-dimensional, steady-state heat balance. The overall heat balance includes a radial thermal conductivity term to account for the effect of a thermal barrier coating on the combustor liner, but axial conduction along the liner is neglected. The resulting heat balance equation is

$$R_1 + C_1 = (KC)_{\text{radial}} = R_2 + C_2 \quad (1)$$

The heat fluxes from the liner to the pressure housing (radiation  $R_2$  and convection  $C_2$ ) could be calculated from

$$R_2 = \frac{\epsilon_w \epsilon_c}{\epsilon_c + \epsilon_w (1 - \epsilon_c) (A_w / A_c)} (T_{WA}^4 - T_c^4) \quad (2)$$

$$C_2 = h_2 (T_{WA} - T_c) \quad (3)$$

where

$$h_2 = 0.02 \frac{K_{an}}{D_{an}} (Re)_{an}^{0.8} (Pr)_{an}^{0.33} \quad (4)$$

The radial heat flux conducted through the liner wall from the flame to the annulus air is calculated using

$$(KC)_{\text{radial}} = \frac{K_{\text{eff}}}{\delta_{\text{eff}}} (T_{WH} - T_{WA}) \quad (5)$$

$$\frac{K_{\text{eff}}}{\delta_{\text{eff}}} = \frac{1}{\delta_{\text{cerm}}} \frac{K_{\text{cerm}}}{K_{\text{Hast}}} + \frac{\delta_{\text{Hast}}}{K_{\text{Hast}}} \quad (6)$$

The convective heat flux from the film-cooling air (hot-gas side) to the liner wall can be written as

$$C_1 = h_1 (T_f - T_{WH}) \quad (7)$$

$$h_1 = 0.023 \frac{K_f}{D_{fi}} (Re)_f^{0.8} (Pr)_f^{0.4} \quad (8)$$

with  $Re$  and  $Pr$  calculated at film conditions.

The film air temperature used above was determined by using the techniques given in Ref. 10,

$$F = \frac{T_H - T_F}{T_H - T_{an}} = \frac{1}{1 + C_m (x/M_s)} \quad (9)$$

The mass flux ratio is

$$M = \rho_s U_s / \rho_H U_H \quad (10)$$

Following the recommendation of Ref. 10,  $C_m = 0.05$ .

The final parameters required to establish the overall heat fluxes to and from the liner and, hence, the liner temperature are the radiative heat transfer from the hot gases to the liner  $R_1$  and the hot-gas temperature  $T_H$ . Both of these parameters could be determined from the radiation measurements. The hot-gas temperature could be determined as in Ref. 6, from the spectral measurement of carbon dioxide band radiation (around  $4.5 \mu\text{m}$ ). The incident flame radiation  $R_1$  could be determined from the measured total flame radiation as follows:

$$R_1 = \alpha_w R_{\text{measured}} \quad (11)$$

This equation adjusts the radiant heat flux to account for the absorptivity of the thermal barrier coating on the combustor liner. The empirical correction of the wall absorptivity used in the heat-transfer analysis of Ref. 9 was found to overpredict the amount of radiation absorbed by the liner. A much more satisfactory agreement with data was obtained using  $\alpha_w = 0.4$  as derived from Ref. 11.

### Results and Discussion

Spectral and total flame radiation measurements were taken at several axial locations in a tubular can combustor. In the following sections, these spectral or total flame radiation measurements are labeled as primary, secondary, or tertiary zone data. Figure 6 shows the relationship between spectral and total measurements taken in the three combustion zones.<sup>§</sup>

<sup>§</sup>The spectral flame radiance was integrated to determine a flame radiation level for the measured  $1.5\text{--}5.5 \mu\text{m}$  wavelength spectrum. Using the spectral radiance around  $4.5 \mu\text{m}$  (as noted earlier), a flame temperature was calculated and this permitted a determination of the flame emissivity for the measured spectral region. This flame emissivity was assumed to be equal to that for the entire electromagnetic spectrum and from this a total flame radiation level could be determined using the spectral measurement. Typically, the measured spectrum covered 70% of the total radiative energy available so that the corrections applied were not large.

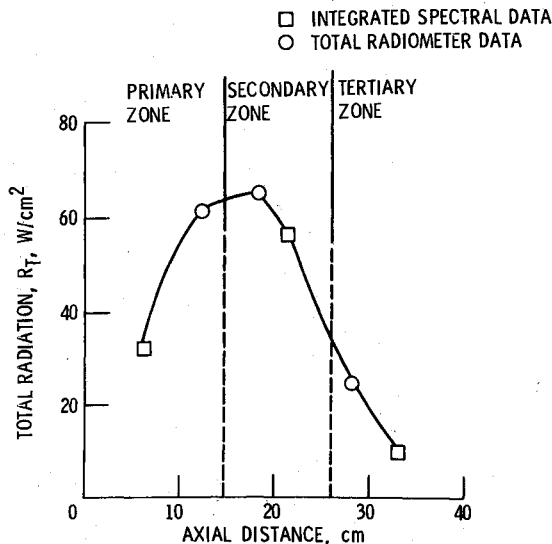


Fig. 6 Total flame radiation as a function of axial combustor distance.

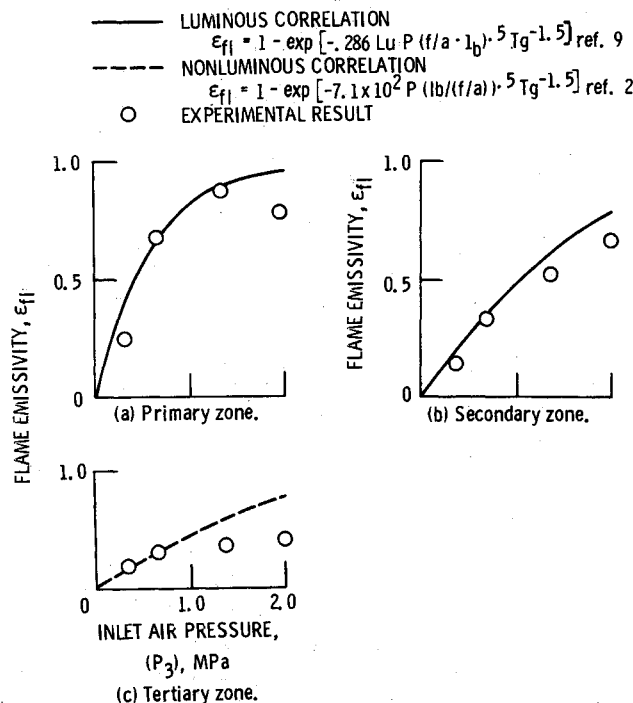


Fig. 7 Comparison of predicted flame emissivity with experimentally measured values (from spectral measurements taken in combustor at three axial locations) as a function of inlet air pressure (533 K inlet air temperature, 0.016 fuel-air ratio, Jet A fuel).

The spectral and total radiation measurements were taken at different axial locations and, accordingly, the two instruments indicate dissimilar flame radiation levels in the combustor. To further complicate matters, these instruments used different fields of view: 0.9 rad for the total radiometer and 0.3 mrad for the spectral radiometer. However, Fig. 6 does show a reasonably good comparison between the two types of measurements.

The variation in flame radiation along the length of the combustor shown in Fig. 6 can be associated with the combustion process. In the primary zone, the high burning zone equivalence ratio ( $\phi > 1$ ) results in rapid soot formation. In the secondary zone, high flame temperatures resulting from near-stoichiometric burning are coupled with large amounts of soot produced in the primary zone, thereby providing the highest

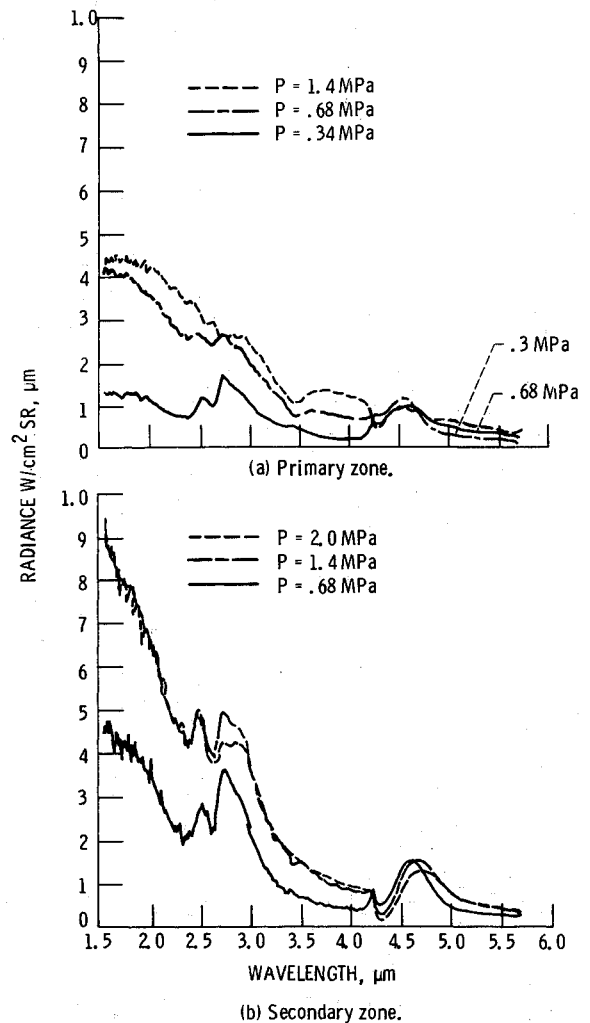


Fig. 8 Spectral flame radiance as a function of inlet air pressure and wavelength for Jet A fuel at inlet air temperature of 534 K and fuel-air ratio of 0.016.

measured levels of flame radiation. The soot formed in the primary zone is oxidized due to the addition of excess air combined with high flame temperatures. In the tertiary zone, dilution air lowers both the soot concentration and hot-gas temperature, thus decreasing the flame radiation level.

In the subsequent sections of this report, the effects of several combustor operating parameters on flame radiation are examined. Note that the spectral and total flame radiation data will not always quantitatively follow the same trends due to the factors discussed above. It should also be noted here that all of these measurements are "path averaged" over the field of view within the combustor. Both axial, radial, and circumferential variations in the soot concentration and gas temperature will effect the measurements displayed in the following sections.

#### Effect of Inlet Air Pressure

Figure 7 reveals the effect of combustor inlet air pressure on flame emissivity as determined from spectral radiance measurements. As expected, flame emissivity increases with inlet air pressure, but the way in which it increases is unique for each combustion zone. In the secondary zone, there is a steep increase in flame emissivity with inlet pressure. In the tertiary zone, however, flame emissivity increases but levels off around 1.5 MPa. In the primary zone, the flame emissivity increases up to a pressure of about 1.5 MPa and then decreases slightly.

A possible explanation for this decrease in flame emissivity at high pressures can be found in an examination of the fuel nozzle spray. At high-pressure levels, the fuel nozzle, operating at a high-pressure drop, injects a finely atomized spray that results in the rapid evaporation of the fuel droplets. In the fuel-rich primary zone, the additional fuel vapor may dilute those reactions occurring close to the fuel nozzle and thus cause lower levels of flame temperature and soot concentration.

Figure 7 also displays curves corresponding to the empirical flame emissivity correlation of Lefebvre.<sup>9</sup> For the primary and secondary zones, the luminous flame radiation correlation matched well with the experimental data up to approximately 1.5 MPa. At the highest inlet air pressure (2.0 MPa), there was a discrepancy of 15-25% between predicted and actual flame emissivity values. As noted above, this discrepancy may be related to the operating characteristics of the fuel nozzle.

In the tertiary zone, flame emissivity data was compared to a nonluminous correlation.<sup>2</sup> A disparity again arises at the higher pressure levels. This may be ascribed to the fact that the empirical correlation was derived principally from low-pressure data.

Figure 8 shows spectral radiance vs wavelength for some representative inlet air pressures. In the primary zone (Fig.

8a), the gas-band radiance at 2.7 and 4.5  $\mu\text{m}$  is easily discernible from the continuum soot spectra only at the 0.34 MPa condition. (Gases radiate over discrete wavelength intervals called "gas bands." In the spectral curves, these appear as increases in radiance around 2.4-3.0 and 4.3-4.7  $\mu\text{m}$ .) At the higher pressure conditions, the gas bands progressively merge with the soot spectra, becoming very nearly a blackbody spectra.

The high-pressure primary zone spectral curves (Fig. 8a) indicate an absorption band around 3.4  $\mu\text{m}$  that becomes more apparent as inlet air pressure is increased. Since hydrocarbons have an absorption band around 3.4  $\mu\text{m}$ , it is possible that cool fuel vapor/droplets cause this absorption in the fuel-rich primary zone. Apparently, this band is not very intense and is prominent only at high pressures.

The spectral radiance is more intense in the secondary zone (Fig. 8b), due primarily to an increase in flame temperature. The gas-band radiance is visible at all pressures due to lower levels of soot concentration. From 0.68 to 1.4 MPa, the spectral radiance steadily increases with inlet pressure, except for the gas-band region around 4.5  $\mu\text{m}$  where the spectral radiance remains constant. This implies a steady increase in the optical density for a constant combustion zone flame temperature. At 2.0 MPa, the data follow a different trend. The 4.5  $\mu\text{m}$  gas-band radiance decreases, indicating a reduction in the flame temperature, while the soot spectra are unchanged from the 1.4 MPa pressure levels. Again, a consideration of the fuel spray nozzle may provide an explanation for this circumstance. At 2.0 MPa, the finely atomized spray may be fully or nearly

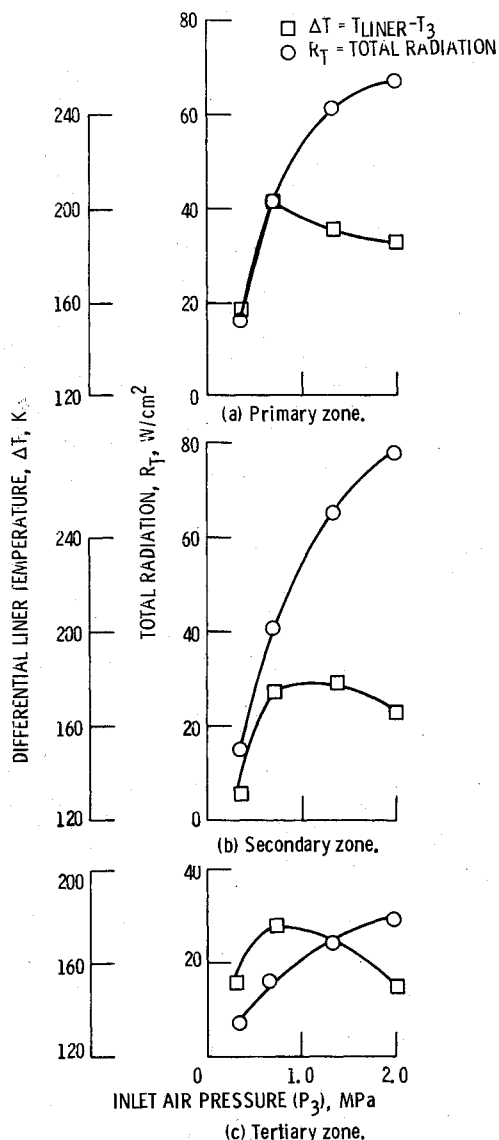


Fig. 9 Total radiance and differential liner temperatures as a function of inlet air pressure at different axial locations (534 K inlet air temperature, 0.016 fuel-air ratio, Jet A fuel). Measurements  $R_T$  made using total radiometers.

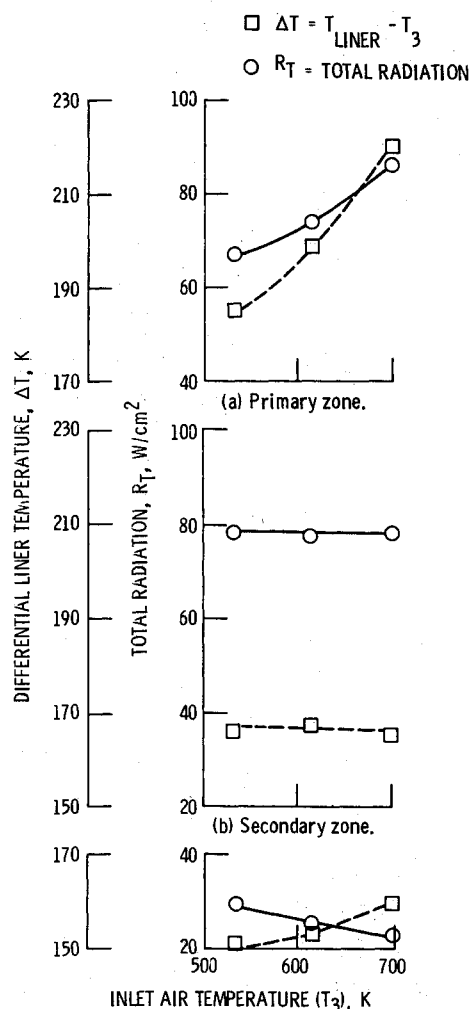


Fig. 10 Differential liner temperature and total radiance as a function of inlet air temperature at three different axial locations (2.0 MPa inlet air pressure, 0.016 fuel-air ratio, Jet A fuel). Measurements  $R_T$  made using total radiometers.

combusted as it reaches the secondary zone. Under these conditions, a sheet of stoichiometrically combusting droplets will not be viewed by the spectral radiometer, resulting in lower measured flame temperatures.

This phenomenon indicated the importance of the fuel spray. Spectral flame radiance measurements obtained with a different fuel nozzle<sup>12</sup> gave evidence of a steady rise in the optical density with a constant flame temperature at the same operating conditions. This variability of flame radiation trends with differing fuel nozzles is more fully examined in Ref. 6.

The effect of inlet air pressure on total flame radiation and local average liner temperature is shown in Fig. 9. As noted previously, the flame radiation decreases with the inlet air pressure, but this same trend is not followed by the local liner temperatures. For example, in the secondary zone an increase in inlet air pressure from 0.7 to 2.0 MPa results in a near doubling of the flame radiation intensity from 41 to 78 W/cm<sup>2</sup>, while the local average liner temperature actually decreases about 10K. Similar trends are seen in the primary and tertiary zone data. The decrease in liner temperatures as the pressure is increased is due to an increase in the effectiveness of convective cooling. This will also be examined in the subsection on liner heat transfer.

#### Effect of Inlet Air Temperature

Figure 10 demonstrates the effect of inlet air temperature on total flame radiation and local differential liner temperature. In the primary zone (Fig. 10a), the total flame radiation increases from 67 to 86 W/cm<sup>2</sup> as the inlet air temperature rises from 533 to 700 K. For this same inlet air temperature in-

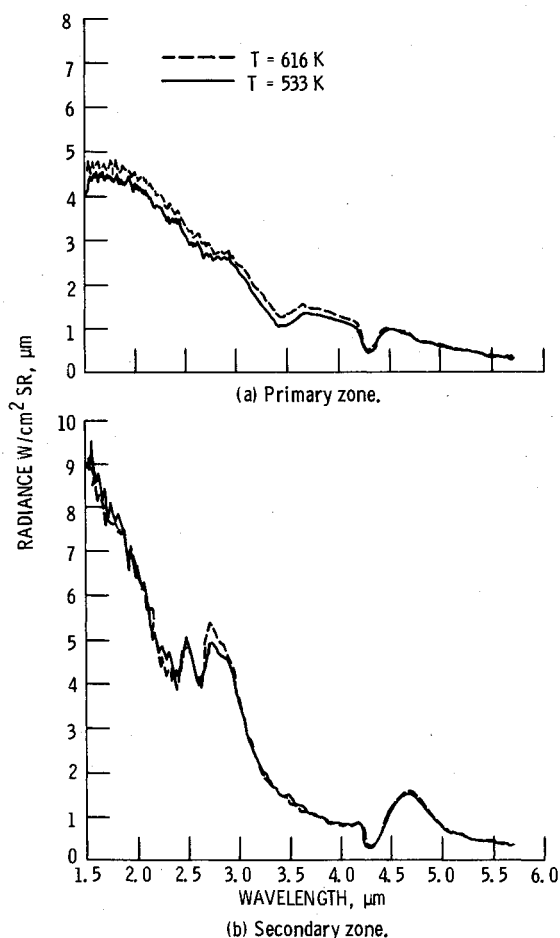


Fig. 11 Spectral flame radiance as a function of inlet air temperature and wavelength for Jet A fuel at inlet air pressure of 1.4 MPa and fuel-air ratio of 0.016.

crease, the local differential liner temperatures increase from 185 to 220 K. In the secondary zone (Fig. 10b), the total flame radiation and differential liner temperatures remain constant with respect to the inlet air temperature. In the tertiary zone (Fig. 10c), the flame radiation decreases linearly with increasing inlet air temperature, an indication of greater soot oxidation. Conversely, differential liner temperatures rise with increasing inlet air temperature. The convective heat-transfer coefficients decrease by about 15% as the inlet air temperature increases from 533 to 700 K. The heat transfer to the cooling air would then be less efficient and lead to the observed higher differential liner temperatures.

Spectral radiance curves for inlet air temperatures of 616 and 533 K are shown in Fig. 11 for the primary and secondary zones. In the primary zone (Fig. 11a), the high-temperature spectral curve is approximately a constant increment more intense than the low-temperature curve over the measured spectrum. This suggests that radiation levels in the primary zone increase not because of higher flame emissivity, but because of higher hot-gas temperatures. In the secondary zone (Fig. 11b), the 616 K spectral curve is more intense around the 2.7 and 4.6 μm gas bands, indicating a higher hot-gas temperature. The soot spectra appear to be unaffected by the inlet air temperature increase. Taken together, these trends indicate that at higher air temperatures the flame emissivity decreases an incremental amount to offset the increase in the hot-gas temperature. This supports the insensitivity of the total flame radiation with respect to inlet air temperature seen in Fig. 10b).

#### Effect of Fuel Type

The effect of a variation in fuel type on total flame radiation is shown in Fig. 12. In the primary and secondary zones (Figs. 12a and 12b), the ERBS fuel emitted discernibly higher levels of flame radiation with the largest percentage increases occurring at the lowest inlet air pressures. For example, in the primary zone at 0.34 MPa, ERBS fuel emitted 56% higher flame radiation levels than Jet A, while at 2.0 MPa the in-

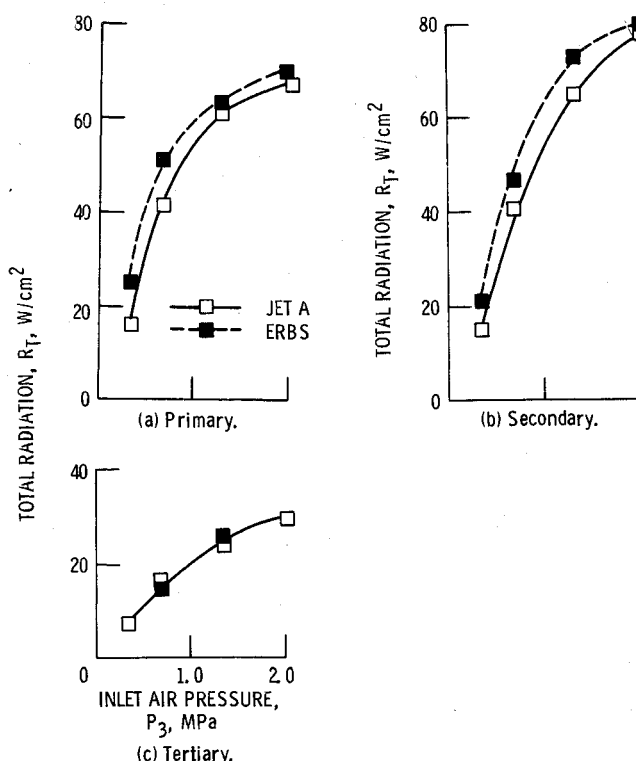


Fig. 12 Total flame radiance as a function of fuel type and inlet air pressure (534 K inlet air temperature 0.016 fuel-air ratio). Measurements  $R_T$  made using total radiometers.

crease was only approximately 6%. In the tertiary zone, the fuel variation resulted in no discernible change in the flame radiation levels.

The spectral radiance curves shown in Fig. 13 further substantiate these trends. In the primary zone at 0.34 MPa (Fig. 13a), the intensity of the gas-band radiance around  $4.5 \mu\text{m}$  remains approximately constant, while the soot continua is more intense with ERBS fuel, indicating higher soot concentration levels. A similar trend is seen in the secondary zone (Fig. 13c) and, to a lesser extent, in the tertiary zone (Fig. 13e). At a higher pressure (0.7 MPa), the primary zone again indicates the presence of higher soot levels, but the secondary and tertiary zones display almost no change in the soot spectra and, hence, concentration levels. Apparently, at the higher pressures the additional soot is oxidized.

### Liner Heat Transfer

The variation of total flame radiation levels between the two different fuel types provided a parametric variation in the liner heat-transfer environment that can be used to estimate the heat loadings to the liner. Effectively, the only variable changing in the heat-transfer environment is the radiative heat flux. The flame temperature (i.e., the gas-band radiance level around  $4.5 \mu\text{m}$  in Fig. 11) appears to be nearly unaffected; therefore, any change in liner temperature should be due only to the variation in the flame radiation levels.

Differential liner temperatures resulting from ERBS and Jet A combustion are compared in Fig. 14a. The variation in total flame radiation levels that cause this liner temperature increase is shown in Fig. 14b. In Fig. 14c, the percentage increase in differential liner temperatures is shown to correspond very strongly with the percentage increase in flame radiation levels.

If the data in Fig. 14 are used as an input to a heat-transfer analysis (described previously), the heat loadings to the combustor liner can be calculated. These calculated heat loads are shown in Fig. 15a as a function of inlet air pressure. The dashed line indicates the heat loadings for ERBS combustion with the solid lines designating Jet A combustion. A somewhat surprising result of this calculation is that the hot-side convec-

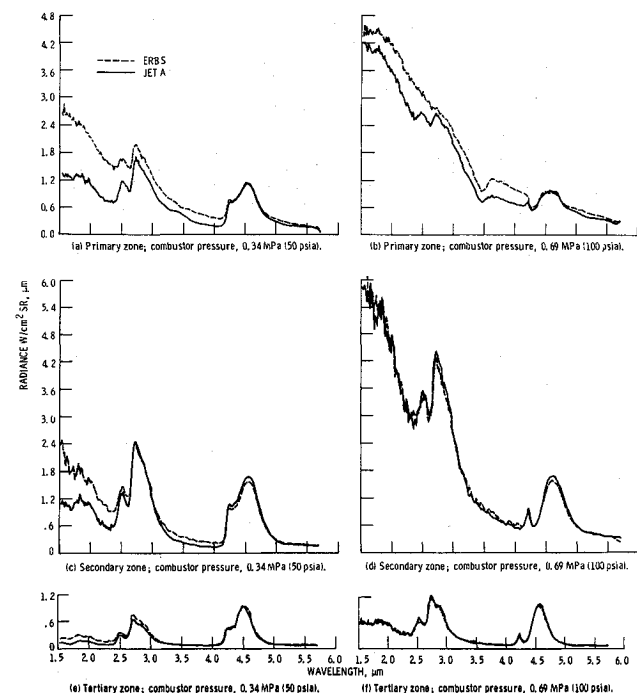


Fig. 13 Variation in spectral flame radiance with spectral wavelength 0.016 fuel-air ratio, Jet A and ERBS fuels, 533 K (500°F) inlet air temperature.

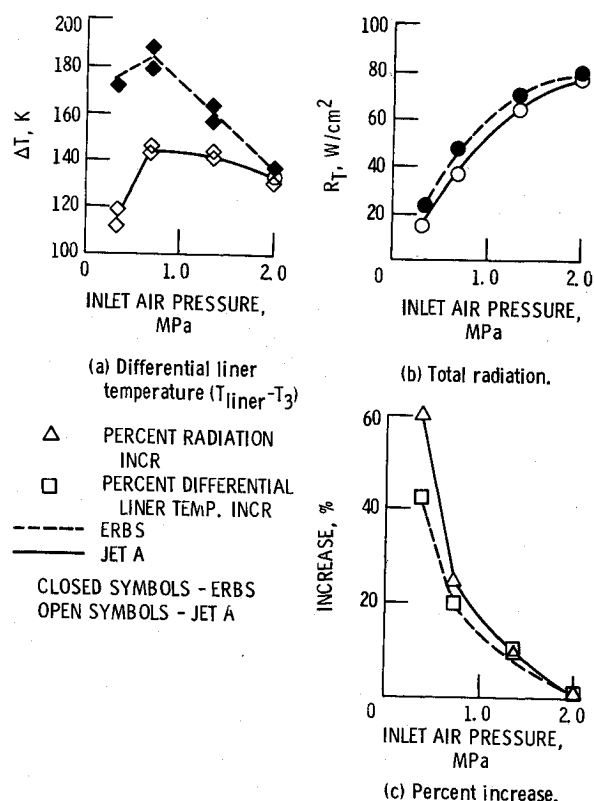


Fig. 14 Differential liner temperature, total flame radiance and percent increase as a function of inlet air pressure (533 K inlet air temperature, secondary zone data, 0.016 fuel-air ratio). Measurements  $R_T$  made using total radiometers.

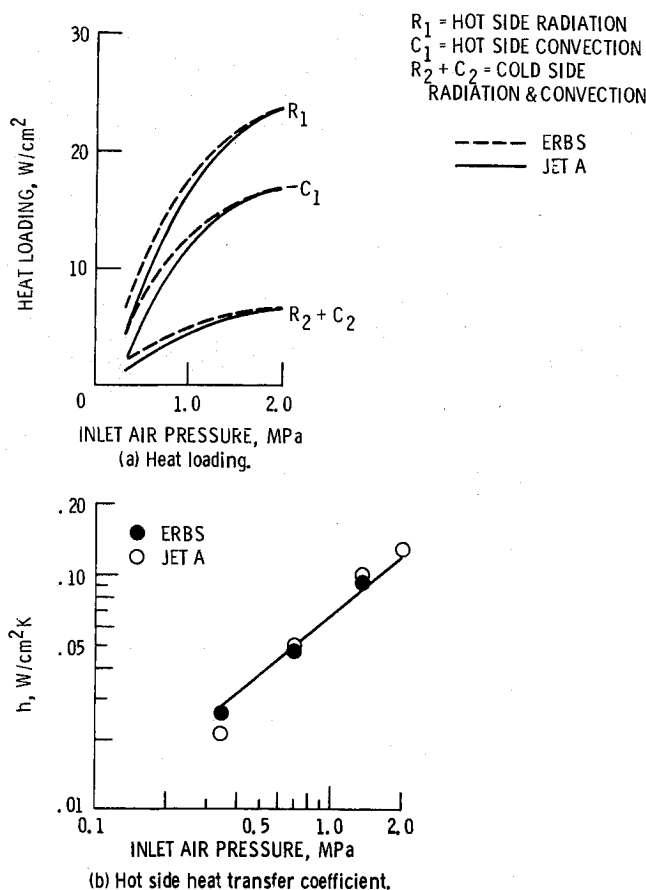


Fig. 15 Calculated heat loads and heat transfer coefficients  $h$  as a function of inlet air pressure.

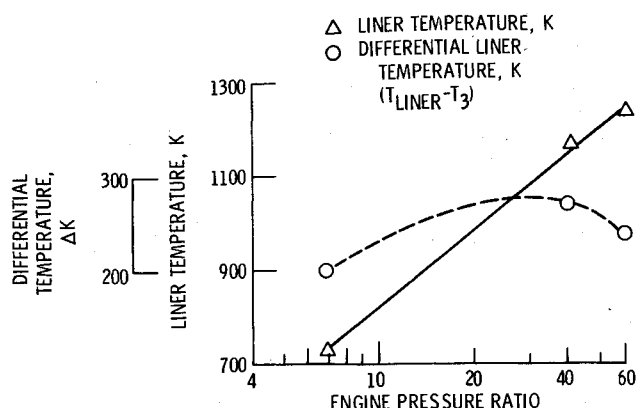


Fig. 16 Predicted differential and liner temperatures as a function of engine pressure ratio.

tive heat flux  $C_l$  is in a negative direction away from the liner. (In this case the negative refers to the definition of  $C_l$ .  $C_l$  is defined as positive when heat is transferred from the film air to the liner. The opposite occurs here.) This effectively reduces the heat flux through the liner to the level of  $R_2$  and  $C_2$ , the backside radiative and convective heat fluxes, respectively. It should be noted that this analysis was made at an axial location along the liner where the film cooling efficiency was high. At different axial locations, the heat fluxes will change and  $C_l$  might become positive.

The method proposed in the section on heat-transfer analysis is typically used for calculating liner temperatures. If, however, the liner temperatures are fixed at the values indicated in Fig. 14 and the hot-side heat-transfer coefficient  $h_l$  is used as the dependent variable, the variation of  $h$  with pressure can be compared with the theoretical variation predicted from Eq. (8). This comparison between theory and experiment is made in Fig. 15b. This comparison between theory and experiment is excellent with the largest variation appearing at the low-pressure conditions.

The fidelity with which  $h_l$  was calculated across the investigated pressure range provides some confidence that this heat-transfer analysis can be extended to examine the impact of advanced cycle engines on liner temperatures. The main difficulty involved in this extension is the determination of the incident radiative heat flux. All previous calculations were able to employ measured radiation values; however, the higher inlet air temperatures and pressures inherent in advanced cycle engines were beyond the experimentally measured range. An extrapolation procedure was used to account for these changes.

The main effect of pressure is to increase the flame emissivity. At an inlet air pressure of 2.0 MPa, flame emissivities fell in a range of 0.7-0.8 in either the primary or secondary zone (Fig. 6). Estimating an extrapolation to higher pressures, the flame emissivity was chosen to be 1.0.

The main effect of higher inlet air temperature was to increase the flame temperature. To extrapolate to higher inlet air temperatures, the measured radiation levels were increased by a factor accounting for the increase in the adiabatic flame temperature. This factor was then combined with the pressure correction to yield an estimated radiation flux. This flux was then inserted into the heat-transfer analysis.

A heat balance was then calculated at three different engine cycle conditions. The lowest pressure ratio condition,  $PR = 7$ , corresponded with the experimentally measured conditions and was used to insure that the analysis could match an engine cycle condition. The higher cycle conditions,  $PR = 40$  and  $60$ , required the radiation level extrapolations. The resulting calculated liner temperatures vs engine pressure ratio are displayed in Fig. 16. The liner temperature at an engine

pressure ratio of 40, approximately 1170 K, is only marginally acceptable for currently used liner metal alloys. At an engine pressure ratio of 60, the nearly 1240 K liner temperatures would be totally unacceptable for durability. An interesting feature of these heat balance calculations is the reduction in differential liner temperature at higher engine pressure ratios, as is shown in Fig. 16. This reduction of differential liner temperature is due to the increased effectiveness of the convective cooling occurring at higher pressures. The absolute liner temperatures still increase since the inlet air temperature is increasing faster than the differential temperature is decreasing. This trend, however, leads to the speculation that for some other liner cooling scheme relying more heavily on convective cooling, the increase in convective cooling efficiency might offset the increase in inlet air temperature and maintain reasonable liner temperature levels. The only other alternative would be to employ higher temperature alloys or ceramics in advanced cycle engines.

### Summary of Results

Total and spectral radiation measurements were made in a tubular-can combustor at a series of parametric operating conditions. From these measurements, the following results were obtained:

- 1) The increase in luminous flame emissivity vs pressure is reasonably well represented by the empirical flame emissivity of Lefebvre.<sup>9</sup> Discrepancies arise mainly at the higher pressure conditions (around 2.0 MPa) and may be associated with fuel injector performance variations.

- 2) An increase in inlet air temperature (from 533 to 700 K) resulted in higher radiation levels in the fuel-rich primary zone and an insignificant change in radiation levels in the secondary zone. Spectral flame radiance measurements indicated that the increased primary zone radiation resulted from the increase in flame temperature occurring at the higher inlet air temperatures. In the secondary zone, the increase in flame temperature was accompanied by a decrease in soot concentration levels, resulting in the invariance of flame radiation with inlet air temperature.

- 3) Combustion of ERBS fuel, a fuel with both a higher viscosity and higher boiling point than conventional Jet A fuel, generally resulted in higher levels of flame radiation than Jet A. The difference in radiation levels was less notable at higher inlet air pressures and at large axial distances from the fuel injector. The higher flame radiation levels are attributable to higher soot levels.

- 4) An extrapolation of the current data to a hot-gas environment representative of a 60:1 pressure ratio engine resulted in calculated average liner temperatures of 1240 K. This temperature is too severe from a durability standpoint indicating a need for improved materials or more effective cooling schemes.

### References

- <sup>1</sup>Sturgess, G. J., "Gas Turbine Combustor Liner Durability," *Gas Turbine Design Problems*, edited by A. H. Lefebvre, Hemisphere Publishing Co., New York, 1980, pp. 133-148 (discussion, pp. 148-150).
- <sup>2</sup>Reeves, D., "Flame Radiation in an Industrial Gas Turbine Combustion Chamber," National Gas Turbine Establishment, England, NGTE-memo-285, 1956.
- <sup>3</sup>Schirmer, R. M. and Quigg, H. T., "High Pressure Combustor Studies of Flame Radiation as Related to Hydrocarbon Structure," Phillips Petroleum Co., Bartlesville, Okla., Rept. 3952-65R, 1965 (AD-617191).
- <sup>4</sup>Jackson, T. A. and Blazowski, W. S., "Fuel Hydrogen Content as an Indicator of Radiative Heat Transfer in an Aircraft Gas Turbine Combustor," AFAPL-TR-79-2014, 1979 (AD-A067709).



<sup>5</sup>Najjar, Y. A. H. and Goodger, E. M., "Radiation and Smoke from the Gas Turbine Combustor Using Heavy Fuels," ASME Paper 81-HT-21, 1981.

<sup>6</sup>Humenik, F. M., Claus, R. W., and Neely, G. M., "Parametric Study of Flame Radiation Characteristics of a Tubular-Can Combustor," ASME Paper 83-JPGC-GT-11, 1983.

<sup>7</sup>Claus, R. W., "Spectral Flame Radiance from a Tubular Can Combustor," NASA TP-1722, 1981.

<sup>8</sup>Seng, G. T., "Characterization of an Experimental Referee Broadened Specification (ERBS) Aviation Turbine Fuel and ERBS Fuel Blends," NASA TM-82883, 1982.

<sup>9</sup>"The Design and Development of Gas Turbine Combustors, Vol. I, Component Theory and Practice," Northern Research and Engineering Corp. Cambridge, Mass., NREC Rept. 1344-2, 1980.

<sup>10</sup>Marek, C. J., "Effect of Pressure on Tangential-Injection Film Cooling in a Combustor Exhaust Stream," NASA TM X-2809, 1973.

<sup>11</sup>Liebert C. H., "Emittance and Absorptance of NASA Ceramic Thermal Barrier Coating System," NASA TP-1190, 1978.

<sup>12</sup>Claus, R. W., Humenik, F. M., and Neely, G. M., "Flame Radiation Measurements," *Combustion Fundamentals Workshop*, NASA CP-2268, 1983, pp. 199-206.

## *From the AIAA Progress in Astronautics and Aeronautics Series*

# **SPACECRAFT RADIATIVE TRANSFER AND TEMPERATURE CONTROL—v. 83**

*Edited by T.E. Horton, The University of Mississippi*

Thermophysics denotes a blend of the classical engineering sciences of heat transfer, fluid mechanics, materials, and electromagnetic theory with the microphysical sciences of solid state, physical optics, and atomic and molecular dynamics. This volume is devoted to the science and technology of spacecraft thermal control, and as such it is dominated by the topic of radiative transfer. The thermal performance of a system in space depends upon the radiative interaction between external surfaces and the external environment (space, exhaust plumes, the sun) and upon the management of energy exchange between components within the spacecraft environment. An interesting future complexity in such an exchange is represented by the recent development of the Space Shuttle and its planned use in constructing large structures (extended platforms) in space. Unlike today's enclosed-type spacecraft, these large structures will consist of open-type lattice networks involving large numbers of thermally interacting elements. These new systems will present the thermophysicist with new problems in terms of materials, their thermophysical properties, their radiative surface characteristics, questions of gradual radiative surface changes, etc. However, the greatest challenge may well lie in the area of information processing. The design and optimization of such complex systems will call not only for basic knowledge in thermophysics, but also for the effective and innovative use of computers. The papers in this volume are devoted to the topics that underlie such present and future systems.

*Published in 1982, 529 pp., 6×9, illus., \$35.00 Mem., \$55.00 List*

TO ORDER WRITE: Publications Dept., AIAA, 1633 Broadway, New York, N.Y. 10019